INNSPUB

International Journal of Biosciences | IJB |
ISSN: 2220-6655 (Print), 2222-5234 (Online)
http://www.innspub.net
Vol. 15, No. 5, p. 548-561, 2019

RESEARCH PAPER OPEN ACCESS

Structural, spectral and bioactivity scores of 5,6 Dimethyl 1-H benzotriazole monohydrate: experimental and DFT study

R. Mini[1,2], T. Joselin Beaula[2], P. Muthuraja[3], V. Bena Jothy[1*]

[1]*Department of Physics and Research Centre, Women's Christian College, Nagercoil 629 001, Tamil Nadu, India*

[2]*Department of Physics and Research Centre,Malankara Catholic College, Kaliakkavilai, Tamil Nadu, India*

[3]*Post graduate and Research Department of Chemistry, Sri Ramakrishna Mission Vidyalaya College of Arts and Science, Coimbatore - 641020, Tamil Nadu, India*

[4]*Affiliated to Manonmaniam Sundaranar University, Abishekapatti, Tirunelveli - 627 012, Tamil Nadu, India*

Key words: DMBM; HOMO-LUMO; DFT; NBO; UV.

http://dx.doi.org/10.12692/ijb/15.5.548-561 Article published on November 28, 2019

Abstract

Bioactive molecules are chemical molecules which produced by living organism that exert a biological effect on other organisms. Benzotriazole derivatives are nitrogen containing bicyclic ring structure and have been confirmed for many biological activities, such as antibacterial, antifungal, anticancer, anti-inflammatory, analgesic, antimalarial and antitubercular activity. In the present work throws different derivatives of benzotriazole and their related to biological activity. Benztriazole derivatives have effectively confirmed as antimicrobial activity. Bioactive molecule 5,6 Dimethyl 1-H Benzotriazole Monohydrate (DMBM) has been performed by the basis set of B3LYP/6-31(d,p) using DFT. Global minimum energy of 5,6 Dimethyl 1-H Benzotriazole Monohydrate is -551.095102444 a.u. Inter and intra-molecular hydrogen bonding are discussed by using Natural Bond Orbital (NBO) analysis. This result has the existence of strong N_3....H_{15}-O_{13} whose energy is about 0.11 kJ/mol which supports the inter-molecular hydrogen bonding. Energy gap between the HOMO and the LUMO is 0.19891 eV. Natural Coordinate Analysis (NCA) has been used as the tool for Spectral interpretations. Red shifting by ~54 cm^{-1} ascribed the level of inter-molecular N-H...O hydrogen bonding. Highly effective inhibition against *Salmonella paratyphi* with a zone diameter of 20mm. Optical transmittance has been performed using UV-visible absorption spectra. The maximum absorption and transmittance peak in the UV–vis spectrum predicts electronic transitions at 199 nm and 243 nm.

* **Corresponding Author:** V. Bena Jothy ✉ benaezhil@yahoo.com

Introduction

Dimethyl 1-H Benzotriazole Monohydrate (DMBM) has been used in large quantities for the production of many industrial chemicals. It is a widely used organic building block in chiral catalysts, ligands, and reagents. Hydroxybenzotriazole is also used for the synthesis of amides from carboxylic acids aside from amino acids. For instance, amide derivatives of ionophoric antibiotics have been prepared [Andrew G. Myers *et al,* 2004, Łowicki & Daniel *et al*, 2009].

The triazole antifungal drugs benzotriazole is used in chemical photography as a restrainer and fog suppressant. Due to spreading resistance of plant pathogens towards fungicides of the strobilurin class, [Gisi *et al*, 2002] control of fungi such as *Septoria tritici* or *Gibberella zeae* [Klix *et al*, 2007] relies heavily on triazoles. Food like store-bought potatoes, contain retardants such as triazole or tetcyclacis. [Mantecón *et al,* 2009] 5,6 Dimethyl 1-H Benzotriazole (DMBM) Monohydrate is a biologically active compound.

In the present study, structural analysis has been performed by density functional theory (DFT) methods B3LYP/6-31(d,p) basis set using Gaussian '09 package. Optical transmittance has been performed using UV-visible absorption spectra.

Natural Bond Orbital (NBO) analysis confirms inter and intra-molecular hydrogen bonding and Charge analysis also analyzed, all these studies are detailed given below.

Methodology

Experimental details

FT-IR of DMBM was recording using the Perkin Elmer FT-IR Spectrometer instrument. FT-Raman spectrum was recorded using the Bruker RFS-27 stand-alone FT-Raman spectrometer instrument. An air-cooled Nd: YAG laser at 1064 nm with an output of 150 mW was used as the exciting source. UV–visible absorption spectrum of solid material has been measured in JASCO (V-570) UV/VIS/NIR spectrometer.

Computational details

DFT computation has been performed using Gaussian'09 program package with B3LYP as the standard 6-31G (d) basis set. Atomic natural charges have been performed by the NBO method using B3LYP 6-31G (d) basis set. Vibrational spectral analysis has been carried out using NCA which is written by Sundius[Sundius 2002]. Electronic properties have been determined by time-dependent DFT (TD-DFT) approach. Important quantities such as electronegativity, hardness, softness, and electrophilicity index have also been deduced (Parr *et al.*, 1983; Kohn *et al.*, 1996& Politzer *et al.*, 1998).

Results and discussion

Optimized geometry

Molecular structure of DMBM was optimized at the B3LYP/6-31G (d) basis set. Optimized geometrical parameters such as bond lengths, bond angles and dihedral angles of DMBM are presented in Table 1 in accordance with the atom numbering scheme given in Fig.1.Angles C_6-C_7-C_{10} is 119° and C_8-C_7-C_{10} is 119° which are slightly out of perfect trigonal angle 120° which is due to the substitution of a methyl group. The dihedral values of N_2-N_3-C_4-C_9 angle is 179° and H_{17}-C_6-C_7-C_8 angle is 179° which is around 180°which confirms the phenyl ring found to be near planar.

The geometry of O_{13}...H_{15} has the distance 1.9128 Å which is significantly shorter than the van der Waals separation between the O atom and the H atom and indicates the strong N-H...O intermolecular hydrogen bonding interaction. Computed values for the bond length N_3-H_{15} of DMBM is 1.018 Å which are lesser than the standard value (1.1Å) indicating charge transfer from H to O of monohydrate by the formation of strong N-H...O intermolecular hydrogen bonding. Generally, C-C bond length is about 1.399Å but bond lengths for C_4-C_5, C_4-C_9, C_5-C_6, and C_7-C_8 are which are longer (above 1.4 Å) than characteristic single bond atoms due to lone-pair-lone-pair repulsion involving two adjacent nitrogen atoms. Among these bond lengths, C_7-C_8 is very high (1.434Å) because of delocalization of charge in the methyl groups.

Table 1. Optimized bond length (Å) Bond angle (°) and Dihedral angle (°) of DMBM.

Bond length	Theoretical (Å)	Bond Angle	Theoretical (Å)	Dihedral Angle	Theoretical (Å)
N1-N2	1.2917	N2-N1-C5	108.3544	C5-N1-N2-N3	0.0007
N1-C5	1.3785	N1-N2-N3	109.1824	N2-N1-C5-C4	0.0004
N2-N3	1.3588	N2-N3-C4	110.392	N2-N1-C5-C6	-179.9997
N3-C4	1.3628	N2-N3- H 15	118.9385	N1-N2-N3-C4	-0.0016
N3-H15	1.0188	C4-N3- H15	130.6695	N1-N2-N3- H15	-179.9969
C4-C5	1.4034	N3-C4-C5	103.4973	N2-N3-C4-C5	0.0017
C4-C9	1.4005	N3-C4-C5	134.8363	N2-N3-C4-C9	179.9997
C5-C6	1.4019	C5-C4-C9	121.6664	H15-N3-C4-C5	179.9963
C6-C7	1.3854	N1-C5-C4	108.5739	H15-N3-C4-C9	-0.0057
C6- H17	1.084	N1-C5-C6	131.1289	N2-N3-O13- H12	62.1299
C7-C8	1.4347	C4-C5-C6	120.2972	N2-N3-O13- H14	-62.3792
C7-C10	1.5105	C5-C6-C7	118.9239	C4-N3-O13- H12	-117.8488
C8-C9	1.3878	C5-C6- H17	120.0253	C4-N3-O13- H14	117.6421
C8-C11	1.5099	C6-C6- H17	121.0508	N3-C4-C5-N1	-0.0013
C9- H16	1.084	C6-C7-C8	120.3102	N3-C4-C5-C6	179.9988
C10- H18	1.0912	C6-C7-C10	119.8257	C9-C4-C5-N1	-179.9996
C10- H19	1.0951	C8-C7-C10	119.864	C9-C4-C5-C6	0.0004
C10- H20	1.0951	C7-C8-C9	120.8698	N3-C4-C9-C8	-179.9985
C11- H21	1.0949	C7-C8-C11	119.7941	N3-C4-C9- H16	0.0027
C11- H22	1.0913	C9-C8-C11	119.3361	C5-C4-C9- H16	-0.007
C11- H23	1.0949	C4-C9-C8	117.9325	N1-C5-C6-C7	-179.9996
H12-O13	0.9632	C4-C9-16	121.4929	N1-C5-C6- H17	180.0
O13- H14	0.9632	C8-C9-16	120.5747	C4-C5-C6-C7	0.0005
O13- H15	1.9128	C7-C10- H18	110.8049	C4-C5-C6- H17	-0.0001
		C7-C10- H19	111.7627	C5-C6-C7-C8	-179.9995
		C7-C10- H20	111.7624	C5-C6-C7-C10	0.0
		H18-C10- H19	107.7224	H17-C6-C7-C8	180.0
		H18-C10- H20	107.7219	H17-C6-C7-C8	179.9995
		H19-C10- H20	106.8467	C6-C7-C8-C11	-0.0005
		C8-C11- H21	111.5805	C10-C7-C8-C9	-0.0003
		C8-C11- H22	111.0285	C10-C7-C8-C11	180.0
		C8-C11- H23	111.5806	C6-C7-C10- H18	179.9997
		H21-C11- H22	107.8365	C6-C7-C10- H19	0.0
		H21-C11- H23	106.766	C6-C7-C10- H20	0.0039
		H22-C11- H23	107.8369	C8-C7-C10- H18	120.1572
		H12-O13- H14	105.6098	C8-C7-C10- H19	-120.1486
		H12-O13- H15	116.5458	C8-C7-C10- H20	-179.9961
		H14-O13- H15	116.6086	C7-C8-C9-C4	-59.8428
				C7-C8-C9- H16	59.8428
				C11-C8-C9-C4	59.8514
				C11-C8-C9- H16	0.0006
				C7-C8-C11- H21	179.9995
				C7-C8-C11- H22	-179.9997
				C7-C8-C11- H23	-0.0008
				C9-C8-C11- H21	59.6763
				C9-C8-C11- H22	-179.9957
				C9-C8-C11- H23	120.3332

Natural bond orbital analysis

NBO analysis has been used to elucidate inter and intra-molecular hydrogen bonding and intermolecular charge transfer. The second order perturbation analysis of the Fock matrix of DMBM using NBO basis are tabulated in Table 2.

Table 2. Second order perturbation analysis of Fock matrix of DMBM using NBO basis.

Donor	ED(i) (e)	Acceptor	ED(j) (e)	E(2)[a] (KJ/mol)	E(j)-E(i)[b] (a.u)	F(ij)[c] (a.u)
σ(N1-N2)	1.98645	σ*(C5-C6)	0.02053	4.01	1.48	0.069
π(N1-N2)	1.90531	π*(N1-N2)	0.42431	0.61	0.32	0.014
		π*(C4-C5)	0.47434	4.09	0.37	0.072
σ(N1-C5)	1.98462	σ*(N2-N3)	0.04380	0.70	1.16	0.026
		σ*(C4-C9)	0.02061	2.95	1.34	0.056
		σ*(C6-C7)	0.01853	0.86	1.39	0.031
σ(N2-N3)	1.99024	σ*(N3-C4)	0.03620	0.91	1.32	0.031
		σ*(C5-C6)	0.02053	0.58	1.42	0.026
σ(N3-C4)	1.98819	σ*(N1-C5)	0.03102	0.61	1.31	0.025
		σ*(N3-C15)	0.03701	0.93	1.24	0.031
		σ*(C4-C5)	0.47434	1.31	1.39	0.046
σ(N3-H15)	1.98839	σ*(N1-N2)	0.00883	2.16	1.20	0.068
σ(C3-C4)	1.96202	σ*(C4-C9)	0.02061	4.60	1.23	0.048
		σ*(C6-H17)	0.01522	2.15	1.12	0.048
		σ*(C9-H16)	0.01560	2.63	1.10	0.066
π(C4-C5)	1.58689	π*(C6-C7)	0.27921	17.31	0.30	0.058
σ(C4-C9)	1.97278	σ*(C8-C9)	0.01922	3.25	1.30	0.061
σ(C5-C6)	1.97485	σ*(C4-C5)	0.47434	3.77	1.25	0.068
σ(C6-C7)	1.97267	σ*(N1-C5)	0.03102	4.87	1.18	0.067
π(C6-C7)	1.73142	π*(C8-C9)	0.2990	19.36	0.29	0.057
σ(C6-H17)	1.97929	σ*(C4-C5)	0.47434	3.77	1.07	0.040
σ(C10-H19)	1.97946	σ*(C6-C7)	0.01853	1.82	1.11	0.040
σ(C11-H21)	1.97824	σ*(C8-C9)	0.01922	1.82	1.10	0.061
σ(C11-H22)	1.98963	σ*(C7-C8)	0.03267	4.34	1.05	0.040
σ(C11-C23)	1.94825	σ*(C8-C9)	0.01922	1.82	1.10	0.063
n(1)N1	1.93179	σ*(C4-C5)	0.47434	5.27	0.94	0.068
n(1)N2	1.95560	σ*(N1-C5)	0.01302	6.29	0.92	0.056
σ(O13-H14)	1.99905	π*(N3-H15)	0.03701	0.11	1.20	0.011

Hyper-conjugation may be given as stabilizing effect that arises from an overlap between an occupied orbital with another neighbouring electron deficient orbitals of DMBM.

Non-covalent bonding (antibonding) interaction is quantitatively described. Lone pair interaction between nitrogen moiety to CN moiety n1 (N2) →σ*(N1-C5) obtained as 6.29 kJ/mol, serves as an evidence for intra-molecular charge transfer interactions from nitrogen moiety. NBO analysis has the existence of strong N3....H15-O13 whose energy is about 0.11 kJ/mol which supports the inter-molecular hydrogen bonding.

HOMO LUMO energy analysis

HOMO and LUMO energies are calculated using the B3LYP/6-31G (d) method and the atomic compositions of the HOMO and LUMO are shown in Fig.2.

Table 3.HOMO and LUMO energies using TD-DFT method.

TD-DFT/B3LYP/6-31G	Gas
E_{HOMO} (eV)	-6.3484
E_{LUMO} (eV)	-6.5473
$E_{HOMO-LUMO}$Gas (eV)	-5.2512
E_{HOMO-1}(eV)	-6.5473
E_{LUMO+1}(eV)	-1.0617
$E_{HOMO-1-LUMO+1}$ (eV)	-5.4855
E_{HOMO-2}	-7.2039
E_{LUMO+2}	-0.2498
$E_{HOMO-2-LUMO+2}$ gas	-6.9541
Electronegativity χ (eV)	2.6256
Chemical harness η(eV)	2.6256
Softness ζ (eV)	0.1904
Electrophillicity ψ (eV)	1.3128

Table 4.UV-vis excitation energy ΔE and oscillator strength (f) for DMBM.

S.No.	Energy	Wavelength (nm)		Oscillator strength	Major contributions
		Cal	Exp		
1	37425	267		0.1008	HOMO→LUMO(87%)
2	39806	251	243	0.1833	H-1→ LUMO (82%)
3	42006	238		0.0056	H-2→LUMO(98%)
4	44944	222		0.0001	HOMO→L+1(90%)
5	46729	213		0.0001	H-1→L+1(58%), HOMO→L+2(32%)
6	46803	213	199	0.0002	H-1→L+1(32%), HOMO→L+2(57%)

The electronic transition absorption corresponds to the transition from the ground to the first excited state and is described by the electron excitation from the HOMO and the LUMO. The HOMO is located over the Benzotriazole and dimethyl groups and the LUMO is located over the Monohydrate. HOMO→LUMO transition implies an electron density transfer from the benzotriazole group to the Monohydrate molecule.

The calculated energy of HOMO is -6.34841eV and the LUMO is -6.54733eV. The energy gap between the HOMO and the LUMO is 0.19891 eV. This small energy gap is responsible for intermolecular charge transfer, which confirms the biological activity of the molecule. By using HOMO and LUMO energies, the electronegativity, chemical hardness, softness and electrophilicity of the title molecule calculated using TD-DFT method and listed in Table 3.The electronegativity, chemical hardness, softness, and electrophilicity index in the gas phase are 2.6256, 2.6256, -0.1904 and 1.3128 respectively.

These results reveal that this molecule has less hardness and high softness due to the low value of the HOMO–LUMO gap. The calculated value of electrophilicity index describes the biological activity of DMBM.

UV vis spectra

UV–Vis absorption and Transmittance spectra of DMBM recorded in water are shown in Fig. 3 a & b. Molecules allow strong π→π* transition in the UV–visible region with high extinction coefficients. NBO analysis indicates that molecular orbitals are mainly composed of π and σ atomic orbital.

Table 5. Vibrational assignments of DMBM by Normal Coordinate Analysis based on SQMFF calculations.

Observed fundamentals /cm^{-1}		Selective scaled B3LYP/6-31(d)force field	
υ_{IR}	υ_{Raman}	υ_{Cal} cm^{-1}	Assignment with PED (≥10%)
3346w		3346	ν_{AS}OH(100)
3246 s		3246	ν_{SS}OH(79), NH$_{R2}$(20)
3224 s		3224	νNH$_{R2}$(78), ν_{SS}OH(19)
		3166	νCH$_{R1}$ (97)
3157 s		3158	νCH$_{R1}$ (99)
	3135vs	3129	ν_{SS}CH$_3$(83),ν_{IS}CH$_3$(16)
3078 w		3093	ν_{OS}CH$_3$(65), ν_{IS}CH$_3$(27)
	3060 w	3054	ν_{IS}CH$_3$(74), ν_{OS}CH$_3$(19)
3045 s		3050	ν_{OS}CH$_3$(100)
		3036	ν_{SS}CH$_3$(74)
		3035	ν_{SS}CH$_3$(31),ωC4(21),τ_{R2}(19),ν_{SS}CH$_3$(12)
3000 w		3001	ν_{IS}CH$_3$(57), ν_{SS}CH$_3$(43)
		1716	νCC$_{R1}$(47),νNHOR$_2$(10),νCH$_{R1}$(10)
1657 s	1652 w	1654	βH2O$_{SD}$(53),βH2O$_{R1}$(24),νCC$_{R1}$(12)
1635 s		1648	βH2O$_{SD}$(69), βH2O$_{R1}$(21)
	1593 s	1582	νCC$_{R1}$(27),NH$_{R2}$(21),NHO$_{R2}$(12)
1544 w		1536	νCC$_{R1}$(33), CH$_{R1}$(28)
	1514 s	1503	ν_{AO}CH2 (61), ν_{AD}CH2(16)
		1496	ν_{AO}CH2 (30),CC$_{R1}$(11),ν_{AD}CH2(11), NH$_{R2}$(10)
1490 w		1490	ν_{AD}CH2(65), ν_{AO}CH2(25)
1478 w		1476	ν_{AD}CH2(63), ν_{AO}CH2(30)
	1460 s	1464	ν_{AO}CH2(25),CC$_{R1}$(15), ν_{AD}CH2(14)
1422 s		1423	CH2$_{R1}$(56),CH2O$_{R1}$(17),ν_{AO}CH$_3$(15)
		1413	CH2$_{R1}$(55),ν_{AO}CH2(17), CH2O$_{R1}$(15)
	1410 w	1410	CH2$_{R1}$(36), CC$_{R1}$(19), CH2O$_{R1}$(13)
	1360vs	1372	βCC(29), βNNR$_2$(20),NHOR$_2$(13)
1355 s		1347	νCN$_{R1}$(24),νCC$_{R1}$(17),τC3(13),CH2$_{R1}$(10)
	1318 w	1315	νCH$_{R1}$(62)
	1281 s	1288	νCC$_{R1}$(21),CN$_{R2}$(21),βNN$_{R2}$(13),CC(10),τC3(10)
1210 s		1211	νCH$_{R1}$(33),CC(19),νCN$_{R2}$(17),νCC$_{R1}$(14)
1154 s		1152	CC(33),CN$_{R1}$(15)
	1105 s	1103	νNN$_{R2}$(37),NHO$_{R2}$(27),H2O$_{R1}$(10)
		1101	C3$_{R1}$(25),ν_{SD}CH$_2$(10),ωCC$_{R1}$(17),CH2O$_{R1}$(16), ωCH$_{R1}$(10)
1064 w		1069	NN$_{R2}$(32), CC$_{R1}$(21), NHOR(16)
	1051 s	1059	ν_{SD} CH2(34),ωCH$_{R1}$(22),CH2O$_{R1}$(20)
	1035 w	1035	CH2O$_{R1}$(39), ν_{SD}CH$_2$(38)
1019 s		1015	CH2O$_{R1}$(39), ν_{SD}CH$_2$(39),CC$_{R1}$(11)
	1009 s	1006	ωCH$_{R1}$(82)
952 w		948	ωCH$_{R1}$(70)
918 s		912	τCNHO(46),τNOH2(44)
896vs		882	βCC$_{R1}$(29),NHO$_{R2}$(14),CN$_{R1}$(12),CC(11)
	847 w	849	NHO$_{R2}$(29),NH$_{R2}$(24),τC3(16),CC(11)
751 w		762	βCC$_{R1}$(45),CC(23),βC3(21)
	747 w	747	τC4(44),ωCC$_{R1}$(20),τC4(17)
717s		708	τC4O$_{R2}$(45),τC4$_{R2}$(32)
594 s		594	νCC$_{R1}$(24),CN$_{R2}$(16),CC(13),NHO$_{R2}$(10)
494 w		495	τC3(29),νCC$_{R1}$(20),CC(11), H2O(11),RCN(11)
	467w	471	βC3(33),βCN$_{R2}$(13),H2O$_{R1}$(12),CC$_{R1}$(11),NHO(10)
427s		404	ωCC$_{R1}$(53), τC4(22)
378 s		377	τC4$_{R2}$(33),τC4(20), ωCC$_{R1}$(12),τC4O$_{R1}$(11)
	330 w	326	H2OR(55),ν_{SD}H2O(24)
		320	ωCC$_{R1}$(84)
		298	τCNHO(32),τNOH2(28),ωH2O(27)
	266 w	272	H2O$_{R1}$(62),ν_{SD}H2O(27), ωH2O(11)
		234	τC4(56),C3N(11)
	179 w	174	τCH(70), τC4(10)
	146 s	146	νOHB(56),H2OR(25), ν_{SD}H2O(14)
	137vs	138	τCH(54),τC3N(12),τCN3$_{R2}$(11)
	125 w	126	τC3N(21),C(21), τCN3(14), ωCN$_{R2}$(14), τC4(13)
	58 s	64	CNHO(75)
		50	NOH2(58),CNHO(37)
	33 w	35	H2OR(59),ν_{SD}H2O(26),ωH2O(10)
		4	ωCN$_{R2}$(52),τC4$_{R2}$(21),τC4(16)

w-weak; vw-very weak; s-strong; vs-very strong; ν-stretching;β-bending; τ-torsion; ss-symmetric; As-asymmetric; R-rocking; ω-wagging; TW-twisting; SD-symmetric deformation; SC-scissoring; IS-in-plane stretching; AD-asymmetric deformation; R1-Phenyl ring; R2- Triazole ring.

TD-DFT/B3LYP/6-31G (d) calculations have been used to determine the low-lying excited states of DMBM.The calculated excitation energies, absorbance, and oscillator strength (f) for the title molecule were compared with the experimental values are tabulated in Table 4.

Table 6. Antimicrobial effect of DMBM.

Sl.No	Microorganisms	Zone of inhibition (diameter in mm)
1	*Salmonella paratyphi*	20mm
2	*Shigella spp.*	19mm
3	*Staphylococcus aureus*	16mm
4	*Streptococcus pyogenes*	15mm
5	*Klebsiella pneumonia*	14mm

The maximum absorption and transmittance peak in the UV–vis spectrum predicts electronic transitions at 199 nm and 243 nm respectively with an oscillator strength f = 0.1833 & 0.0002 showing good agreement with the characteristic peak that arises in the pyrazine system due to n→π* transition [Mohan et.al, 2009].

Table 7. Definition of internal valence coordinates of DMBM.

Number	Symbol	Type	Definition
			STRETCHING
1-6	ri	CC	C_4-C_5,C_5-C_6,C_6-C_7,C_7-C_8,C_8-C_9,C_9-C_4
7-8	ri	CH	C_9-H_{16},C_6-H_{17}
9-10	ri	CN	C_5-N_1,C_4-N_3
11-12	ri	NN	N_1-N_2,N_2-N_3
13	ri	NH	N_3-H_{15}
14-15	ri	CC1	C_8-C_{11},C_7-C_{10}
16	ri	OH	O_{13}-H_{14}
17	ri	OH1	O_{13}-H_{12}
18- 33	ri	CH1	C_{11}-H_{21},C_{11}-H_{22},C_{11}-H_{23},C_{10}-H_{18},C_{10}-H_{19},C_{10}-H_{20},C_{11}-H_{21},C_{11}-H_{22},C_{11}-H_{23},C_{10}-H_{18},C_{10}-H_{19},C_{10}-H_{20},C_{11}-H_{22},C_{11}-H_{23},C_{10}-H_{19},C_{19}-H_{20}
34	ri	OH2	O_{13}- H_{15}
			BENDING
35-38	βi	CCH	C_8-C_9-H_{16},C_4-C_9-H_{16},C_7-C_6-H_{17},C_3-C_6-H_{17}
39-42	βi	CCC	C_9-C_8-C_{11},C_7-C_8-C_{11},C_6-C_7-C_{10},C_8-C_7-C_{10}
43	βi	CNH	C_4-N_3-H_{15}
44	βi	NNH	N_2-N_3-H_{15}
45-48	βi	CCN	C_9-C_4-N_3,C_3-C_4-N_3,C_4-C_5-N_1,C_6-C_5-N_1
49-64	βi	CCC1	C_4-C_5-C_6,C_6-C_7-C_8,C_8-C_9-C_4,C_5-C_6-C_7,C_7-C_8-C_9,C_9-C_4-C_5,C_4-C_5-C_6,C_7-C_8-C_9,C_5-C_6-C_7,C_6-C_7-C_8,C_8-C_9-C_4,C_9-C_4-C_5,C_5-C_6-C_7,C_8-C_9-C_4,C_6-C_7-C_8,C_9-C_4-C_5
65-70	βi	HCH	H_{20}-C_{10}-H_{19}, H_{19}-C_{10}-H_{18},H_{20}-C_{10}-H_{18}, H_{22}-C_{11}-H_{23},H_{23}-C_{11}-H_{21},H_{22}-C_{11}-H_{21}
71-76	βi	HCC	H_{20}-C_{10}-C_7, H_{19}-C_{10}-C_7,H_{18}-C_{10}-C_7, H_{22}-C_{11}-C_8,H_{23}-C_{11}-C_8,H_{21}-C_{11}-C_8
77-82	βi	HCH1	H_{20}-C_{10}-H_{19},H_{19}-C_{10}-H_{18},H_{20}-C_{10}-H_{18}, H_{22}-C_{11}-H_{23},H_{23}-C_{11}-H_{21},H_{22}-C_{11}-H_{21}
83-86	βi	HCH2	H_{19}-C_{10}-H_{18},H_{20}-C_{10}-H_{18},H_{23}-C_{11}-H_{21},H_{22}-C_{11}-H_{21}
87-92	βi	HCC1	H_{20}-C_{10}-C_7,H_{19}-C_{10}-C_7,H_{18}-C_{10}-C_7,H_{22}-C_{11}-C_8,H_{23}-C_{11}-C_8,H_{21}-C_{11}-C_8
93-96	βi	HCC2	H_{19}-C_{10}-C_7,H_{18}-C_{10}-C_7,H_{23}-C_{11}-C_8,H_{21}-C_{11}-C_8
97-98	βi	HOH	H_{14}-O_{13}-H_{12},H_{14}-O_{13}-H_{15}
99-100	βi	HOH1	H_{14}-O_{13}-H_{15},H_{12}-O_{13}-H_{15}
101	βi	NHO	N_3-H_{15}-O_{13}
102	βi	CNN	C_4-N_3-N_2
103-104	βi	NNC	N_2-N_1-C_5,N_2-N_1-C_5

105	βi	CCN	C_5-C_4-N_3
106	βi	NCC	N_1-C_5-C_4
107	βi	NNN	N_3-N_2-N_1
108	βi	CCN	C_5-C_4-N_3
109	βi	NNC	N_2-N_1-C_5
110	βi	NCC	N_1-C_5-C_4
		OUT-OF-PLANE BENDING (WAGGING)	
111-112	ωi	CCCH	C_4-C_9-C_8-H_{16},C_5-C_6-C_7-H_{17}
113-114	ωi	CCCC	C_7-C_8-C_9-C_{11},C_8-C_7-C_6-C_{10}
115	ωi	NNCH	N_2-N_3-C_4-H_{15}
116-117	ωi	CCCN	C_5-C_4-C_9-N_3,C_6-C_5-C_4-N_2
118	ωi	HOHH	H_{14}-O_{13}-H_{12}-H_{15}
		TORSION	
119-134	τi	CCCC	C_4-C_5-C_6-C_7,C_6-C_7-C_8-C_9,C_8-C_9-C_4-C_5,C_5-C_6-C_7-C_8,C_7-C_8-C_9-C_4,C_9-C_4-C_5-C_6,C_4-C_5-C_6-C_7,C_7-C_8-C_9-C_4,C_6-C_7-C_8-C_9,C_9-C_4-C_5-C_6,C_5-C_6-C_7-C_8,C_8-C_9-C_4-C_5,C_4-C_5-C_6-C_7,C_6-C_7-C_8-C_9,C_7-C_8-C_9-C_4,C_9-C_4-C_5-C_6
135-136	τi	NHOH	N_3-H_{15}-O_{13}-H_{12},N_3-H_{15}-O_{13}-H_{14}
137-138	τi	CNHO	C_4-N_3-H_{15}-O_{13},N_2-N_3-H_{15}-O_{13}
139-144	τi	CCCH	C_6-C_7-C_{10}-H_{18},C_6-C_7-C_{10}-H_{19},C_6-C_7-C_{10}-H_{20},C_8-C_7-C_{10}-H_{18},C_8-C_7-C_{10}-H_{19},C_8-C_7-C_{10}-H_{20}
145-150	τi	CCCH1	C_7-C_8-C_{11}-H_{21},C_7-C_8-C_{11}-H_{23},C_7-C_8-C_{11}-H_{22}, C_9-C_8-C_{11}-H_{21},C_9-C_8-C_{11}-H_{23},C_9-C_8-C_{11}-H_{22}
151	τi	CNNN	C_4-N_3-N_2-N_1
152	τi	CCNN1	C_5-C_4-N_3-N_2
153	τi	NNNC	N_3-N_2-N_1-C_5
154	τi	NCCN	N_1-C_5-C_4-N_3
155	τi	NNCC	N2-N1-C5-C4
156-157	τi	NHOH	N_3-H_{15}-O_{13}-H_{12},N_3-H_{15}-O_{13}-H_{14}
158-159	τi	CNHO	C_4-N_3-H_{15}-O_{13},N_2-N_3-H_{15}-O_{13}
160-161	τi	CCCN	C_9-C_4-C_5-N_1,C_6-C_5-C_4-N_3

Table 8. Definition of local symmetry coordinates.

Number	Symbol	Definition
	STRETCHING	
1-6	νCC	r_1,r_2,r_3,r_4,r_5,r_6
7-8	νCH	r_7,r_8
9-10	νCN	r_9,r_{10}
11-12	νNN	r_{11},r_{12}
13	νNH	r_{13}
14-15	νCC1	r_{14},r_{15}
16	νOHSS	$(r_{16}+r_{17})/\sqrt{2}$,$(r_{16}-r_{17})/\sqrt{2}$
17-19	νCH1SS	$(r_{18}+r_{19}+r_{20})/\sqrt{3}$,$(r_{26}+r_{27}+r_{28})/\sqrt{3}$,$(2r_{21}+r_{22}+r_{23})/\sqrt{6}$,$(2r_{29}-r_{30}-r_{31})/\sqrt{6}$,$(r_{24}+r_{25})/\sqrt{2}$, $(r_{32}-r_{33})/\sqrt{2}$
20	νOHAS	r34
	BENDING	
21-22	CCH	$(\beta_{35}+\beta_{36})/\sqrt{2}$,$(\beta_{37}+\beta_{38})/\sqrt{2}$
23-24	CCC	$(\beta_{39}+\beta_{40})/\sqrt{2}$,$(\beta_{41}+\beta_{42})/\sqrt{2}$
25	N2H	$(\beta_{43}+\beta_{44})/\sqrt{2}$
26-27	CCN	$(\beta_{45}+\beta_{46})/\sqrt{2}$,$(\beta_{47}-\beta_{48})/\sqrt{2}$
28-30	CCC1D	$(\beta_{49}+\beta_{50}+\beta_{51})/\sqrt{6}$,$(\beta_{52}-\beta_{53}-\beta_{54})/\sqrt{6}$, $(\beta_{55}+\beta_{56}+\beta_{57})/\sqrt{6}$,$(\beta_{58}-\beta_{59}-\beta_{60})$, $(\beta_{61}+\beta_{62}-\beta_{63}-\beta_{64})/\sqrt{4}$
31-32	CH2SS	$(\beta_{65}+\beta_{66}+\beta_{67}-\beta_{68}-\beta_{69}-\beta_{70})/\sqrt{6}$, $(\beta_{71}+\beta_{72}+\beta_{73}-\beta_{74}-\beta_{75}-\beta_{76})/\sqrt{6}$
33-34	CH_21AS	$(2\beta_{77}+\beta_{78}+\beta_{79})/\sqrt{4}$,$(2\beta_{80}-\beta_{81}-\beta_{82})/\sqrt{4}$
35-36	CH_22ASO	$(\beta_{83}+\beta_{84})/\sqrt{2}$,$(\beta$ 85-$\beta_{86})/\sqrt{2}$
37-38	C2HROCK	$(2\beta_{87}+\beta_{88}+\beta_{89})/\sqrt{4}$,$(2\beta_{90}-\beta_{91}-\beta_{92})/\sqrt{4}$

39-40	C2H1ROCKO	$(\beta_{93}-\beta_{94})/\sqrt{2},(\beta_{95}-\beta_{96})/\sqrt{2}$
41	WSS	$(2\beta_{97}+\beta_{98}-\beta_{99})/\sqrt{4}$
42	WROCK	$(\beta_{100}-\beta_{101})/\sqrt{2}$
44	NHO	β_{102}
45	CN2	$\beta_{103},\beta_{104},\beta_{105},\beta_{106},\beta_{107}$
46	N3DO	$\beta_{108},\beta_{109},\beta_{110},\beta_{111}$
	WAGGING	
47	ωC3H	$\omega_{112},\omega_{113}$
48	ωCCC	$\omega_{114},\omega_{115}$
49	ωN2CH	$\omega_{116},\omega_{117}$
50	ωC3N	$\omega_{118},\omega_{119}$
51	ωOH3	ω_{120}
	TORSION	
52-54	τC4	$(\tau_{121}+\tau_{122}+\tau_{123}-\tau_{124}-\tau_{125}-\tau_{126})/\sqrt{6},(\tau_{127}+\tau_{128}-\tau_{129}-\tau_{130})/\sqrt{4},(2\tau_{131}+2\tau_{132}-\tau_{133}-\tau_{134}-\tau_{135}-\tau_{136})/\sqrt{12}$
55	τNH2O	$(\tau_{137}+\tau_{138})/\sqrt{2}$
56	τCNHO	$(\tau_{139}+\tau_{140})/\sqrt{2}$
57-58	τC3H	$(\tau_{141}+\tau_{142}+\tau_{143}+\tau_{144}-\tau_{145}-\tau_{146}-\tau_{147}-\tau_{148})/\sqrt{12}$
59-60	τCN3	$\tau_{149},\tau_{150},\tau_{151},\tau_{152},\tau_{153},\tau_{154}$
61	τCN3O	$\tau_{155},\tau_{156},\tau_{157},\tau_{158},\tau_{159}$
62-63	τC3N	$(\tau_{160}+\tau_{161})/\sqrt{2}$

The wavelengths obtained with B3LYP/6-31G (d) computations are 267 nm, 251 nm, 238 nm, 222 nm, and 213 nm. Both HOMO and LUMO are the main orbitals that take part in chemical stability. In view of calculated absorption and transmittance spectra, the respective wavelengths are 199 and 243 nm. These absorption spectra correspond to the electronic transition from the HOMO-1 to LUMO+1 with 32% contribution as well as HOMO to LUMO+2 with 57% contribution and HOMO-1 to LUMO with 82% contribution respectively.

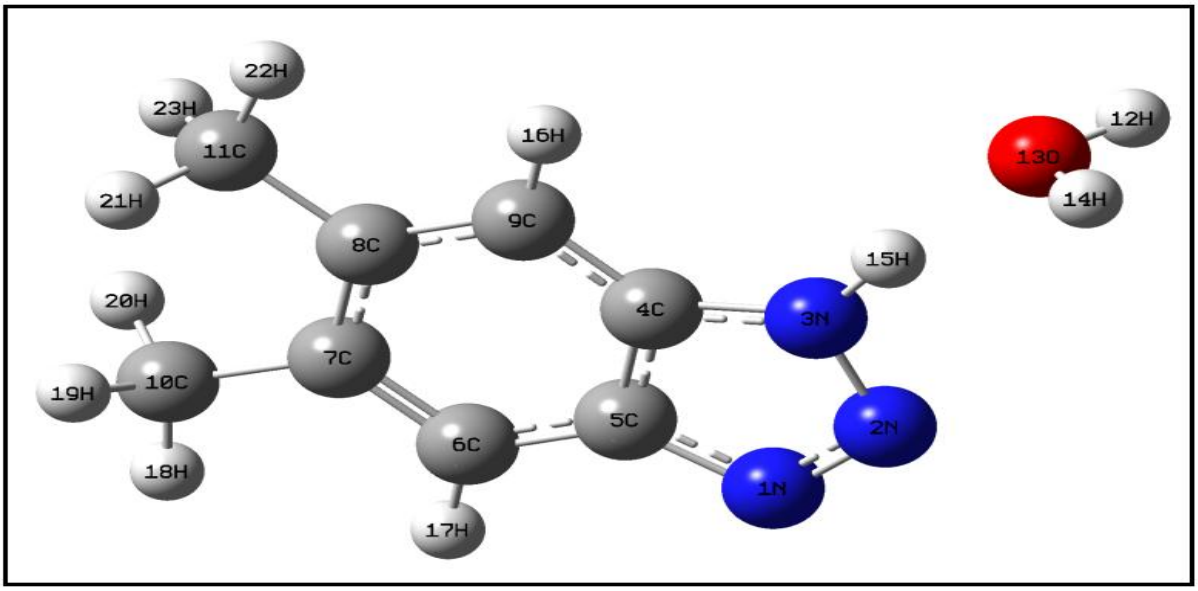

Fig. 1. Optimized molecular structure of DMBM.

Vibrational spectral analysis

Assignments of FT-IR and Raman spectra were carried out with the aid of NCA followed by the force field calculations with the same method that was employed for the geometry optimization of the molecule. A non-redundant set of internal coordinates for DMBM has been defined and used as a data file to MOLVIB program.

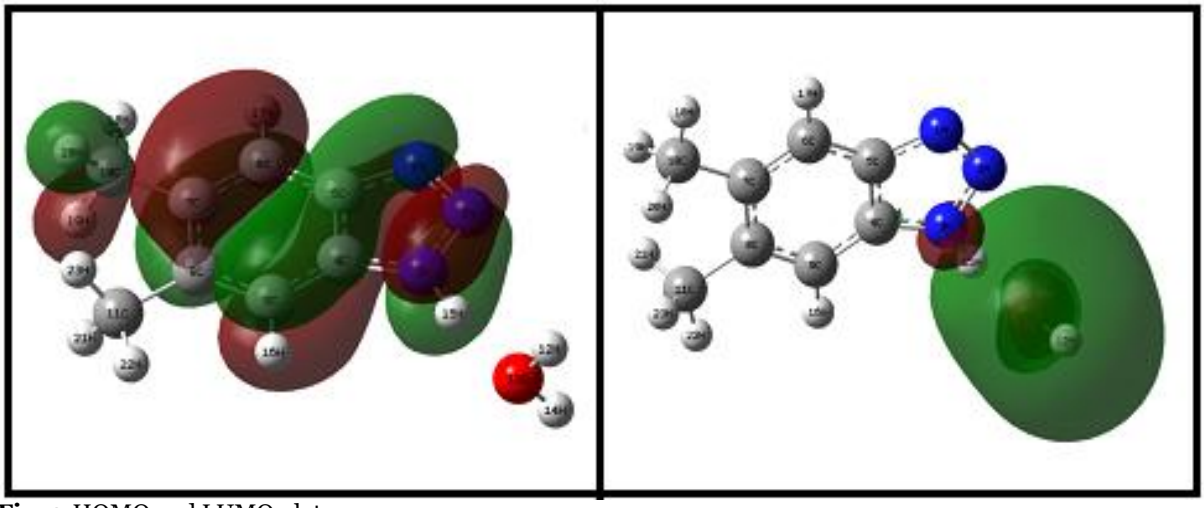

Fig. 2.HOMO and LUMO plots.

The computed wave numbers were selectively scaled using a set of 16 transferable scale factors with an RMS frequency error of 9 cm^{-1}. Experimental and simulated FT-IR and Raman spectra were shown as overlaid with the corresponding simulated spectra Fig.4 and 5 for visual comparisons.

In DMBM have 2 methyl (CH_3) groups and two rings such as Phenyl ring and Triazole ring. These two rings assume the vibrations. Thus, the molecule has C-C stretching, C-H stretching, N-N stretching, N-H stretching, and O-H stretching.

Experimental and calculated frequencies, IR and Raman intensities with the PED contributions have been tabulated in Table 5. The vibrational assignments for different functional groups have been discussed below:

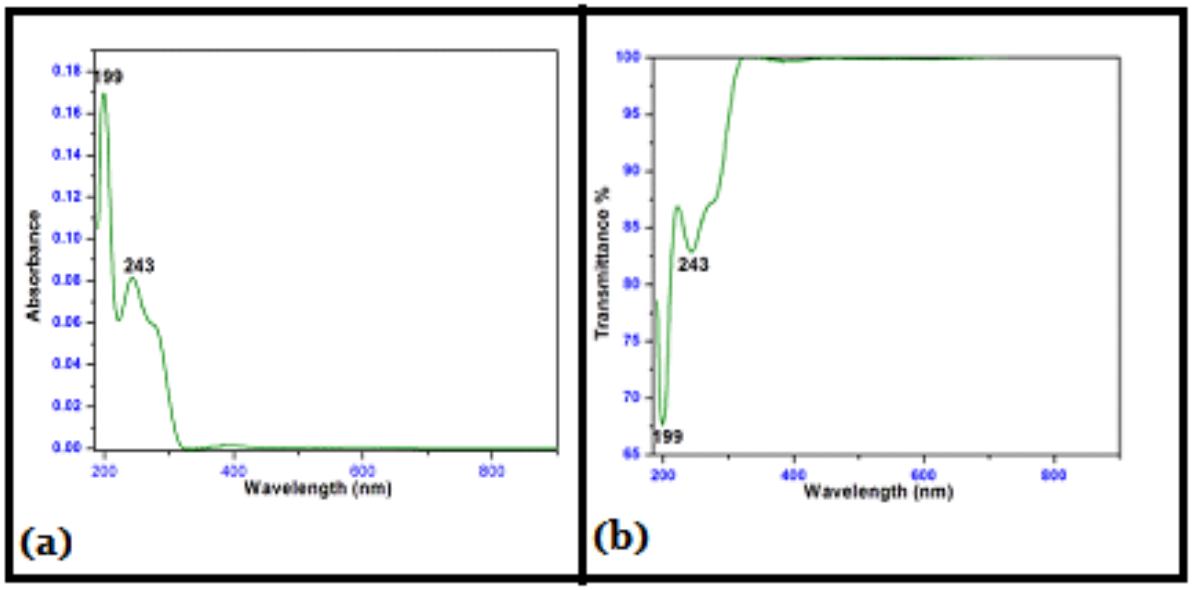

Fig. 3.UV VIS (a) Absorbance (b) Transmittance spectrum of DMBM.

Methyl vibrations

CH_3 group makes significant contributions in the vibrational spectra of MNBA. Symmetric and asymmetric stretching modes of a methyl group attached the benzene ring are usually downshifted due to electronic effects and are expected near 2925 and 2865 cm^{-1} for asymmetric and symmetric stretching vibrations. A symmetric stretching mode is observed as a weak band in Raman at 3060 cm^{-1}. This can direct to changing polarizability and dipole

moment due to electron delocalization. Thus, the hyperconjugation and back donation of the methyl group, causing changes in the intensity in IR spectrum which clearly indicates that methyl hydrogen is directly involved in the donation of electronic change [Smith *et al.*, 1999].

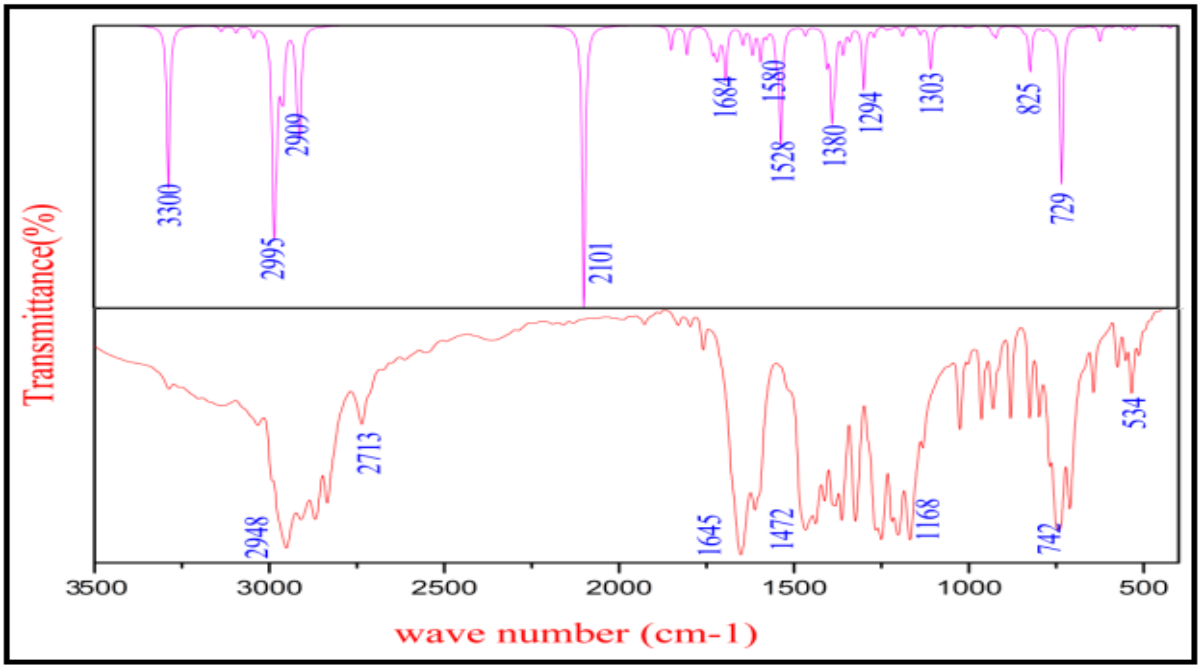

Fig. 4. Experimental and stimulated FT-IR.

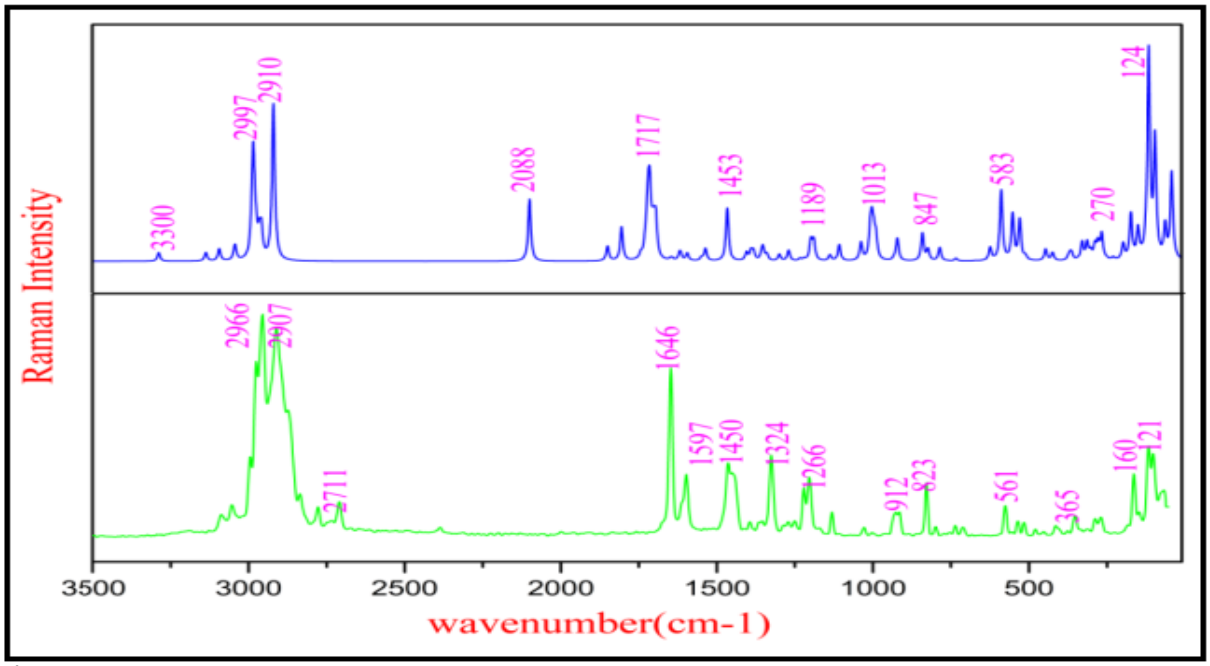

Fig.5. Experimental and stimulated FT-Raman spectra of DMBM.

The methyl group yields the strengthening of C-H bond which is clearly reflected in the experimental value of C-H bond length (Table 1). Generally, the out-of-plane bending mode of the methyl group is expected near 1460 cm^{-1}. CH_3 out-of-plane bending mode is coupled with CH_3 in-plane bending mode and is observed as a strong band at 1422 cm^{-1} in IR spectrum with a major PED contribution of 99% is shown in Table 5. Torsion and other modes are given in Table 7 & 8.

H_2O vibrations

H_2O group makes, O-H stretching band is characterized by the symmetric and asymmetric expected region is 3400-3500 cm^{-1} [Kolesov and Geiger 2000]and it has been observed as a band at 3346 cm^{-1} in IR. Red shifting by ~54 cm^{-1} ascribed the level of inter-molecular N-H...O hydrogen bonding. Theoretically predicted wave numbers 3346 cm^{-1}coincide exactly with the experimental wave numbers and these modes are pure stretching modes as evident from the PED value 100%. Raman band observed at 1652 cm-1 and the strong IR band is 1657 cm^{-1} having the symmetric deformation stretching vibration. Rocking vibration is observed in IR as a strong band at 1657 cm^{-1}. Other modes are observed in Table 5.

Fig. 6. Photographs of DMBM.

Phenyl ring vibrations

Phenyl vibrations are reasonably in good agreement with the DFT wave numbers and the assignments made according to Wilson's numbering convention (Varsanyi *et al.*, 1990). C-C stretching modes are 8a, 8b, 19a, 19b and 14.

The degenerate mode 8a is expected to occur in the region 1570-1628 cm^{-1} and the frequency domain of 8b extends from 1570-1614 cm-1. Strong IR band observed at 1657 cm-1 and a strong band at 1652 cm^{-1} in Raman have been assigned to the degenerate mode 8a. The C-C stretching in Raman at1593 cm^{-1} as a strong band is assigned for 8b mode.

C-C stretching mode 19a is observed in IR as a strong band at 1422 cm^{-1} which is strongly coupled with the C-H bending mode. Another possible C-C stretch vibration of poly-substituted benzene is mode 14, which is observed in Raman as a very strong band at 1360 cm^{-1}. C-H in-plane bending vibrations are usually expected to occur in the region 1000-1300 cm^{-1}. A strong band at 1152 cm^{-1} is observed in the IR spectrum and Raman weak bands are 1064 and 1035 cm^{-1}. All other vibrations are given in Table 5.

Triazole ring vibrations

In hetero-cyclic compounds, N-H stretching vibration occurs in the region 3500–3000 cm^{-1} [Sathyanarayana 2004] and is observed as a shoulder band at 3224 cm^{-1} in IR and scaled value at 3224 cm^{-1} with 78% PED contribution. Normally C-N stretching vibrations of aromatic rings in the region 1382–1266 cm^{-1} [Silverstein and Webster 2003] which is

observed at 1335 cm^{-1} in IR. Scaled values of this mode at 1347 cm^{-1} reveals that these modes are not pure modes but contain a significant contribution from other modes. N-N stretching vibration is observed as a very strong band at 1360 cm^{-1} with scaled value at 1372 cm^{-1}.

Antimicrobial activity

DMBM was tested for its antimicrobial activity against human pathogens of clinical isolates (*Salmonella paratyphi, Shigella sp., Staphylococcus aureus, Streptococcus pyogenes and Klebsiella pneumonia*) are given in Table 6 and Fig.6. These results showed highly effective inhibition against *Salmonella paratyphi* with a zone diameter of 20mm which is followed by *Klebsiella pneumonia, Staphylococcus aureus, Streptococcus pyogenes* and *Shigellaspp*19mm,16mm,15mm,14mm respectively.

Conclusion

In the present study, analyzing the structural properties with DFT computations and the detailed spectral investigations of DMBM has been performed. Vibrational assignments of DMBM has been analysed using IR and FT Raman. Phenyl ring found to be near planar. Due to substitution of methyl group slightly out of perfect trigonal angle 120° of the ring. Hyper conjugation and back donation of methyl group, causing changes in the intensity in IR spectrum which clearly indicates that methyl hydrogen are directly involved in the donation of electronic change.

References

Andrew MyersG, Bryant YangH, Hou Chen. 2000. Transformation of Pseudoephedrine Amides into Highly Enantiomerically Enriched Aldehydes, Alcohols, and Ketones, Organic Syntheses **77,** p 29-37.

Bettye SmithL, Tilman SchäfferE, Mario Viani James, ThompsonB, Neil FrederickA, Johannes Kindt, Angela Belcher, Galen Stucky D, Daniel Morse E, Paul Hansma K.1999. Molecular mechanistic origin of the toughness of natural adhesives, fibres and composites, Nature, **399,** p 761–763.

Gisi U, Sierotzki H, Cook A, Mc Caffery A. 2002. Mechanisms influencing the evolution of resistance to Qo inhibitor fungicides, Pest Management Science **58,** p 859–867.

Jorge MantecónD. 2009. Control of potato early blight with triazole fungicide using preventive and curative spraying, or a forecasting system, Ciencia e Investigación Agraria **36(2),** p 291-296.

Klix MB, Verreet JA, Beyer M. 2007. Comparison of the declining triazole sensitivity of Gibberellazeae and increased sensitivity achieved by advances in triazole fungicide development, Crop Protection **26,** p 683-690.

Kolesov Geiger. 2000. The orientation and vibrational states of H2O in synthetic alkali-free beryl, Physics and Chemistry of Minerals **27(8),** p 557–564.

Leszek Kalinowski, Anna Janaszak-Jasiecka, Anna Siekierzycka, Sylwia Bartoszewska, Marcin Woźniak, Dawid Lejnowski, James, F Collawn, Rafal Bartoszewski. 2016. Posttranscriptional and transcriptional regulation of endothelial nitric-oxide synthase during hypoxia: the role of microRNAs, Cellular & Molecular Biology Letters **21(16).**

Łowicki Daniel Huczyński A, Ratajczak-Sitarz M, Katrusiak A, Stefańska J, Brzezinski B, Bartl F. 2009. Structural and antimicrobial studies of a new N-phenylamide of monensin A complex with sodium chloride, Journal of Molecular Structure, **923,** p 53–59.

Nandini G, Sathyanarayana DN. 2004. Ab initio studies of solvent effect on molecular conformation and vibrational spectra of diacetamide, Spectrochimica Acta Part A: Molecular and Biomolecular Spectroscopy **60(5),** p 1115-1126.

Paul Von Ragué Schleyer. 2001. Introduction: Aromaticity, Chemical Reviews **101(5),** p 1115-1118.

Paul Von Ragué Schleyer. 2005. Introduction: Delocalization Pi and Sigma, Chemical Reviews, **105(10),** p 3433-3435.

Réti F, Bertóti I, Mink G Varsányi G. 1990. On the surface thermodynamics of γ-Al2O3 derived from the reaction with chlorine, Solid State Ionics **44,** p 33-39.

Sathyanarayana DN. 2004. Vibrational Spectroscopy: Theory and Applications, New Age International Publishers, New Delhi.

Silverstein RM, Webster FX. 1998. Spectrometric Identification of Organic Compounds, 6th Edition, John Wiley & Sons, New York.

Silverstein RM, Webster FX.2003, Spectrometric Identification of Organic Compounds, John Wiley and Sons, New York.

Sundius T. 2002. 'Scaling of ab initio force fields by MOLVIB', Vibrational Spectroscopy **29,** p 89-95.